




Article

Synthesis of Zinc Oxide Nanoparticles Using *Rubus fairholmianus* Root Extract and Their Activity against Pathogenic Bacteria

Naresh Kumar Rajendran , Blassan P. George *, Nicolette N. Houreld  and Heidi Abrahamse 

Laser Research Centre, Faculty of Health Sciences, University of Johannesburg, P.O. Box 17011, Doornfontein, Johannesburg 2028, South Africa; naresh.r84@outlook.com (N.K.R.); nhoureld@uj.ac.za (N.N.H.); habrahamse@uj.ac.za (H.A.)

* Correspondence: blassang@uj.ac.za; Tel.: +(27)-11-559-6926; Fax: +(27)-11-559-6448

Abstract: Recently, the biosynthesis of zinc oxide nanoparticles (ZnO NPs) from crude extracts and phytochemicals has attracted much attention. Green synthesis of NPs is cost-effective, eco-friendly, and is a promising alternative for chemical synthesis. This study involves ZnO NPs synthesis using *Rubus fairholmianus* root extract (RE) as an efficient reducing agent. The UV spectrum of RE-ZnO NPs exhibited a peak at 357 nm due to intrinsic bandgap absorption and an XRD pattern that matches the ZnO crystal structure (JCPDS card no: 36-1451). The average particle size calculated from the Debye–Scherrer equation is 11.34 nm. SEM analysis showed that the RE-ZnO NPs spherical in shape with clusters (1–100 nm). The antibacterial activity of the NPs was tested against *Staphylococcus aureus* using agar well diffusion, minimum inhibitory concentration, and bacterial growth assay. The *R. fairholmianus* phytochemicals facilitate the synthesis of stable ZnO NPs and showed antibacterial activity.

Keywords: zinc oxide; green synthesis; nanoparticles; antibacterial; *Rubus fairholmianus*



Citation: Rajendran, N.K.; George, B.P.; Houreld, N.N.; Abrahamse, H. Synthesis of Zinc Oxide Nanoparticles Using *Rubus fairholmianus* Root Extract and Their Activity against Pathogenic Bacteria. *Molecules* **2021**, *26*, 3029.

<https://doi.org/10.3390/molecules26103029>

Academic Editors:
Patrizia Ferraboschi and
Fiorella Meneghetti

Received: 22 April 2021
Accepted: 14 May 2021
Published: 19 May 2021

Publisher's Note: MDPI stays neutral with regard to jurisdictional claims in published maps and institutional affiliations.



Copyright: © 2021 by the authors. Licensee MDPI, Basel, Switzerland. This article is an open access article distributed under the terms and conditions of the Creative Commons Attribution (CC BY) license (<https://creativecommons.org/licenses/by/4.0/>).

1. Introduction

Metal oxide nanoparticles have received remarkable attention in biomedical technology and are extensively used in engineering and medical applications due to their high surface area. Both the metal and metal oxide nanoparticles hold strong antioxidant and antimicrobial properties, which are widely used for the detection of pathogenic microbes and diagnosis of cancer progression [1]. Metal oxide nanoparticles such as zinc (Zn), calcium (Ca), and magnesium (Mg) oxide nanoparticles at a minimum concentration significantly inhibit microbial growth. ZnO-NPs are commonly used in the production of anti-itch creams, anti-septic lotion, anti-microbial powders, anti-bacterial band-aids, surgical tapes, anti-dandruff lotion, diaper powders, and ceramics [2]. Hamelian and colleagues synthesized silver nanoparticles through a green synthesis method using *Thymus kotschyianus* extract as a reducing agent. The synthesized silver nanoparticles showed strong antioxidant and antibacterial but less cytotoxic effects [3]. Hemmati et al. [4] reported the green synthesis of silver nanoparticles using fritillaria flower plant extract as a reducing and capping agent. Various researchers explained the antimicrobial and antioxidant properties of metal nanoparticles, the metal nanoparticles have shown strong antimicrobial properties, in both in vitro and in vivo experiments [5–9].

Among various nanoparticles, ZnO has recently received much attention due to its unique properties (wide and direct bandgap (3.3 eV) and large excitation binding energy (60 meV)). ZnO is highly catalytic in nature with photochemical activity [10]. Generally, ZnO NPs are produced by several physicochemical approaches such as direct homogenous precipitation, hydrothermal and solvothermal reactions, metal decomposition, chemical vapor decomposition, laser irradiation, mechanochemical milling, and molecular

beam epitaxy. The chemical synthesis of ZnO NPs involves the consumption of various organic solvents, oxidizing, and reducing agents that are tedious, expensive, and non-eco-friendly [11]. Hence, there is a need for an alternative approach to synthesize ZnO NPs in an eco-friendly way. In contrast to chemical synthesis, biological nanoparticle synthesis uses microbes, enzymes, fungi, or plants as reducing agents in the production of ZnO NPs [12,13]. Based on previous studies, it is understood that ZnO exhibits significant growth inhibition of a broad spectrum of bacteria [14,15]. Zinc oxide nanoparticles can also be used as a drug delivery vehicle to deliver various drug molecules to the targeted cells [12].

The use of plant and plant-based bioactive compounds for the synthesis of metal nanoparticles is attracting attention due to their excellent reducing capacity and antimicrobial activity and this process is known as green synthesis [15]. In green synthesized nanoparticles, the bioactive/phytochemical compounds present in the plant extract are strongly bound or encased over the surface of nanomaterials that will have both the properties of nanomaterials and phytochemicals. Phytochemicals or plant bioactive compounds, which have strong unique properties of that particular plant (e.g., phenols, vitamins, terpenoids, ketones, aldehydes, and amides), play a pivotal role in treating various diseases. The type of plant and plant extract determines the size and shape of the nanoparticles. The increased biological activity of the green synthesized nanoparticles is due to the synergistic effect of the bioactive compounds present in plants and nanomaterial precursors used for synthesis. The green synthesized nanoparticles have also shown various properties such as electrochemical detection of many antibiotic drugs due to the superior electrochemical performance of biosynthesized nanoparticles [16–18].

In recent years, a lot of interest has been raised in isolating plant-based bioactive compounds using alcoholic extracts to perform pharmacological experiments [19]. The main aim of these pharmacological experiments is to control fungal and bacterial infections in human beings. Various ethnomedical plants (e.g., *Alhaji camelorum*, *Anthemis nobilis*, *Berberis integerrima*, and *Zingiber officinale*) are used for their antibacterial and antifungal properties [20–23]. *R. fairholmianus* is an ethnomedicinally important plant with antioxidant and anticancer properties. Various bioactive compounds were isolated from various *Rubus* species (*Rubus amabilis*, *Rubus niveus*, *Rubus sachalinensis*, *Rubus idaeus*, *Rubus molucanus*, *Rubus ellipticus*, *Rubus brasiliensis*) and the preliminary phytochemical screening showed the presence of phenolic compounds, anthocyanins, terpenoids, flavonoids, terpenoids, polyphenols, and aldehydes. Studies reported that *R. fairholmianus* root acetone extract showed the presence of many phenolic compounds. Cis-2-(isopentyloxycarbonyl) benzoic acid, 2-(5-methylhexyl) benzoic acid, 4-methylpentyl benzoate, 3-(iminomethyl)-2,4-dimethylphenol, and isopentyl benzoate or 3-methyl benzoate are some of the bioactive compounds isolated from *R. fairholmianus*, which showed strong antioxidant properties, active in inhibiting BRCA oncoproteins and COX inflammatory proteins with in vitro anticancer properties against various cell lines [24,25]. Plant phenolic compounds hold significant antioxidant properties, and antioxidants are well known for their metal ion-reducing properties. This action favors the formation of nanoparticles in the green synthesis method. Moreover, the presence of various proteins, lipids, and amino acids in plants supports the formation of nanoparticles and inhibits nanoparticle cluster formation or particle agglomeration. To date, there are no reports on the use of *R. fairholmianus* extracts for the biosynthesis of ZnO NPs. This study is the first report on the synthesis of ZnO NPs through a green chemistry approach using *R. fairholmianus* root extract (RE) as an effective reducing agent, and to evaluate their antimicrobial properties.

2. Materials and Methods

2.1. Plant Collection, Extraction and Biosynthesis of ZnO NPs

R. fairholmianus was collected from Kerala, India, and the authenticity was confirmed (voucher specimen no: BSI/SRC/5/23/2010-11/Tech.1657) by the Botanical Survey of India. The root (100 g) of *R. fairholmianus* was washed under running tap water, dried,

and powdered. The powdered roots were extracted with acetone using Soxhlet apparatus. Then, 200 mg of dried extract was dissolved in 10 mL of 0.5% DMSO [25].

Biosynthesis of NPs was carried out according to the procedure of Zheng et al. [26]. Briefly, 10 mL *R. fairholmianus* root extract in 0.5% DMSO was added into 10 mL of 0.5 M zinc nitrate solution and stirred at 80 °C for 48 h. The pale white precipitate formed after centrifugation (30 min at 2500 rpm) was washed with double distilled water. RE-ZnO NPs were collected by drying at 40 °C in a hot air oven. Meanwhile, to compare the biosynthesized NPs, the ZnO NPs were chemically synthesized using sodium hydroxide according to the method of Zheng et al. [26]. A modified green synthesis protocol for the zinc oxide nanoparticles using various plant extracts is given in Table 1.

Table 1. Biosynthetic conditions of nanoparticles synthesized from various plant extracts.

Plant Name	Biosynthesis Conditions	Nature	References
<i>Mussaenda frondosa</i> L.	Continuous stirring at 70 °C for 15 min + drying at 400 °C 30 min + calcination at 400 °C	Crystal	[27]
<i>Cayratia pedata</i>	Continuous stirring at 65 °C for 20 min + drying at 65 °C for overnight + calcination at 400 °C for 2 h	Fine powder	[28]
<i>Eucalyptus globulus</i> Labill	Continuous stirring at 60 °C for 1 h + drying at 100 °C + calcination 400 °C for 2 h	Fine powder	[29]
<i>Mimosa pudica</i>	Continuous stirring at room temperature for 4 h + drying at 300 °C for 45 min + calcination 400 °C	Crystal	[30]
<i>Beta vulgaris</i> , <i>Cinnamomum tamala</i> , <i>Cinnamomum verum</i> , <i>Brassica oleracea</i> var.	Continuous stirring at 70 °C until white paste formation + calcination 400 °C for 2 h	Coroase powder	[31]

2.2. Characterization of Biosynthesized RE-ZnO NPs

The crystalline structure of RE-ZnO NPs was characterized from 5° to 80° in 2θ by XRD (Panalytical X-PertPro X-Ray Diffractometer with Philips PW1729 diffractometer equipped with Cu Kα radiation source which operates at 45 kV/40 mA). The surface morphology of RE-ZnO NPs was categorized by a TESCAN, VEGA Scanning electron microscope operating at 20 kV and the samples were coated with carbon to acquire higher resolution images. UV-Vis spectrophotometer was used to find the stability of the synthesized RE-ZnO NPs in distilled water and the wavelength used was in the range of 200–800 nm (Schimadzu UV-1208, Kyoto, Japan). Fourier-transform infrared spectroscopy (FTIR) (Perkin-Elmer PE 1600, MA, USA) was used to find out the chemical and functional group of RE and RE-ZnO NPs. For FTIR analysis, the samples were made into pellets using KBr reagent and measured in the spectral range of 400–4000cm⁻¹. Finally, thermal properties of RE-ZnO NPs were measured using thermogravimetry (TGA)/differential scanning calorimeter (DSC) (TGA/DSC-60H Schimadzu, Kyoto, Japan) at a heating rate of 10.0 °C/min at room temperature and at 1000 °C in nitrogen gas to establish the ratio of organic/inorganic contents.

2.3. Agar Well Diffusion Method for Antimicrobial Activity

The agar well diffusion technique was used to find the antibacterial activity of RE-ZnO NPs using *S. aureus* (ATCC® BAA-1026TM). Briefly, a sterile cotton swab was dipped into a broth culture of *S. aureus* (1 × 10⁵ cfu/mL) and spread uniformly on nutrient agar plates. Two agar wells of 5 mm diameter were prepared with the help of a sterilized stainless steel cork borer. About 100 μL of RE-ZnO NPs or RE were added to wells and the plates were incubated at 37 °C for 24 h. Then the zones of inhibition (appearance of clear area/white color area around the wells) and the diameter of each zone of inhibition were measured and the mean values were recorded.

2.4. Minimum Inhibitory Concentrations

The minimum inhibitory concentration (MIC) for *S. aureus* (ATCC[®] BAA-1026[™]) was determined as sensitivity to the synthesized RE-ZnO NPs, RE, and ampicillin (positive control) using the microdilution assay according to Mandell et al. [32]. Twenty-four-hour fresh cultures were prepared and the standardized inoculum was made and used for the antibacterial assay. In brief, a 96-well plate was prepared by dispensing 190 μ L Mueller-Hinton broth (MHB) and 10 μ L inoculum (10^5 CFU/mL) into each well. Various dilutions of RE, RE-ZnO NPs, and ampicillin (1 mg/mL) were mixed with MHB in the microplates containing the previously added inoculums and plates were incubated at 37 °C for 24 h. The well with only MHB served as a blank control. *S. aureus* growth was determined at 590 nm using a microplate reader (Reagen Microplate Reader, NJ, USA).

2.5. Bacterial Growth in Different Concentrations of RE-ZnO NPs

S. aureus (ATCC[®] BAA-1026[™]) suspensions (0.2 mL) were inoculated into corresponding tubes containing 1.5 mL of different concentrations of RE, ZnO NP, and RE-ZnO NPs and 1.5 mL of MHB. To these test tubes, 1 mL of phenol red indicator solution was added. Tubes containing inoculum alone served as positive controls and tubes with RE-ZnO NPs + nutrient media served as negative controls. Test tubes with only MHB served as a blank control and tubes were incubated at 37 °C for 24 h and were observed for change in color and pH.

3. Results and Discussion

The successful biosynthesis of RE-ZnO NPs using *R. fairholmianus* root extract was observed by the change in the color of the reaction solution from a brownish-yellow to a pale white after mixing plant extract with zinc nitrate for 48 hr.

Figure 1 displays the UVs absorption spectrum of the RE and RE-ZnO NPs. A peak was observed at 280 nm, which could be attributed to the $n-\pi^*$ transition of the molecules present in the RE. The spectrum of RE-ZnO NPs revealed a peak at 357 nm due to intrinsic bandgap absorption, which confirms the RE-ZnO NPs synthesis. The bandgap energy was calculated at 3.47 eV [33,34].

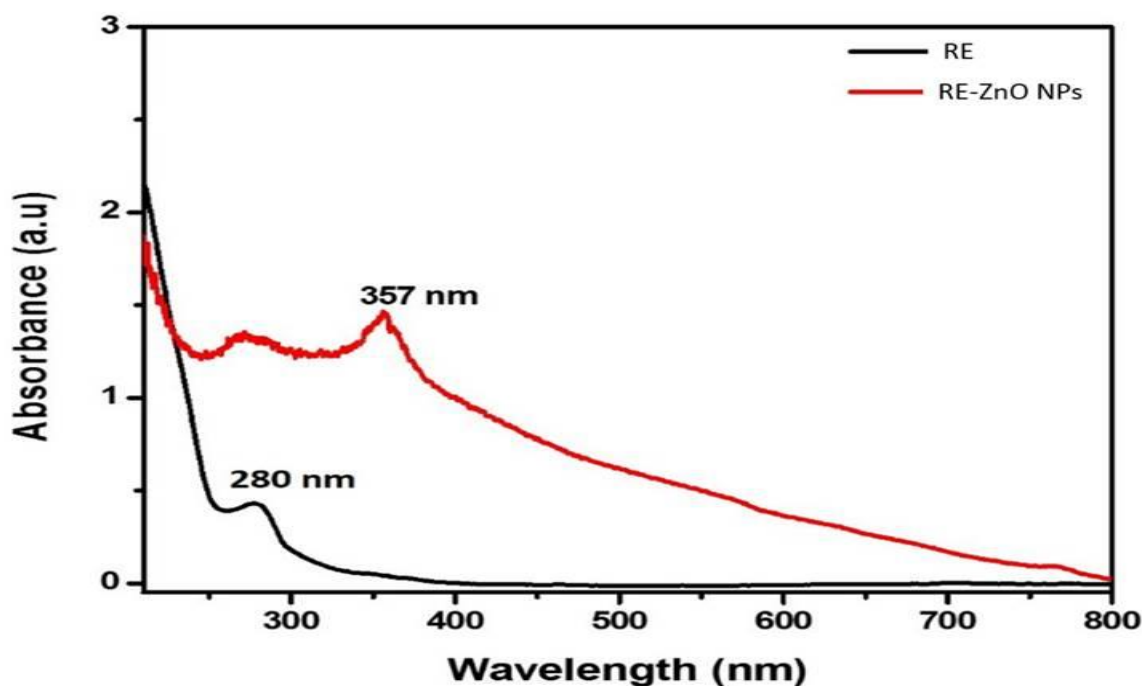


Figure 1. UV-VIS absorption spectra of *R. fairholmianus* root extract (RE) and RE-zinc oxide nanoparticles (RE-ZnO NPs).

Figure 2 shows the FTIR spectrum of the RE and RE-ZnO NPs. The plant extracts showed various functional peak stretches from 3440 cm^{-1} (hydroxide) to 2856 cm^{-1} (carboxyl) groups. Hydrogen bonds (OH) stretched at 3440 cm^{-1} , C-H stretching was observed at 2856 cm^{-1} , COO symmetric stretch was found at 1426 cm^{-1} , and COO asymmetric stretching at 1626 cm^{-1} . Similar types of peaks were also observed in RE-ZnO NPs spectra, which showed a stretching of COO symmetric and asymmetric bonds around $1400\text{--}1600\text{ cm}^{-1}$ and indicating the presence of carboxyl groups over the surface of ZnO NPs. The ZnO peak was observed at 486 cm^{-1} and the presence of phytochemical compounds (polyphenolics, flavonoids, tannins, glycosides, saponins, and gallic acids) in *Rubus* (RE) facilitates the formation of ZnO NPs by acting as a reducing and stabilizing agent. Another reason is that the polyphenolic groups present in *Rubus* also promote the reduction of zinc nitrate to zinc oxide and stabilize the formation of RE-ZnO NPs. These spectral results were consistent with the studies of Senthilkumar et al. [34].

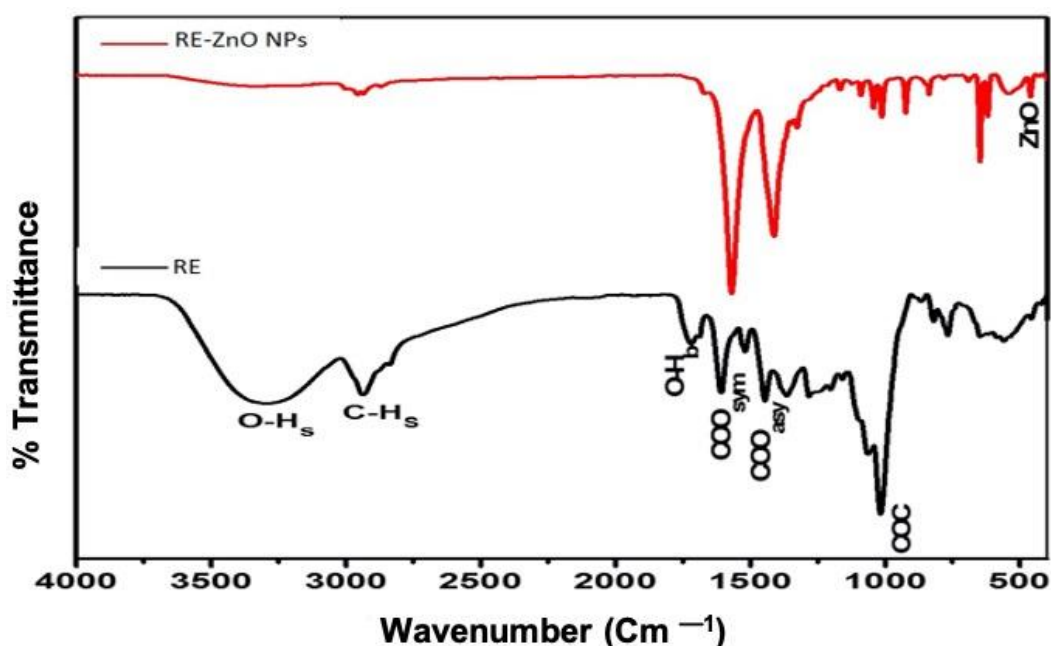


Figure 2. FTIR spectra of *R. fairholmianus* root extract (RE) and RE-zinc oxide nanoparticles (RE-ZnO NPs).

Figure 3a,b describe the TGA/DSC spectra of the RE and RE-ZnO NPs, which displayed heat at $10\text{ }^{\circ}\text{C}/\text{Min}$. TGA was used to decompose the prepared materials, and release water and volatile organic molecules [35,36]. The extract gives three types of weight loss of 26.78%, 11.44%, and 20.88% with corresponding temperatures of $205\text{ }^{\circ}\text{C}$, $604\text{ }^{\circ}\text{C}$, and $789\text{ }^{\circ}\text{C}$, respectively. The weight loss of the extract at 26.78% is due to the removal of water molecules [37]. The weight loss of 11.44% might be due to the decomposition of hydroxide and volatile organic groups [38]. The TGA/DSC spectrum of RE-ZnO NPs is shown in Figure 3b. The DSC curve of RE-ZnO NPs exhibited exothermic and endothermic peaks at $95\text{ }^{\circ}\text{C}$ and $395\text{ }^{\circ}\text{C}$, respectively. The exothermic peak revealed weight loss (1.68%), which is due to the removal of water and organic volatile molecules from the RE-ZnO NPs. The endothermic peak at $395\text{ }^{\circ}\text{C}$ reveals the decomposition of zinc hydroxide to ZnO NPs with the weight loss (0.93%), as shown in Figure 3b.

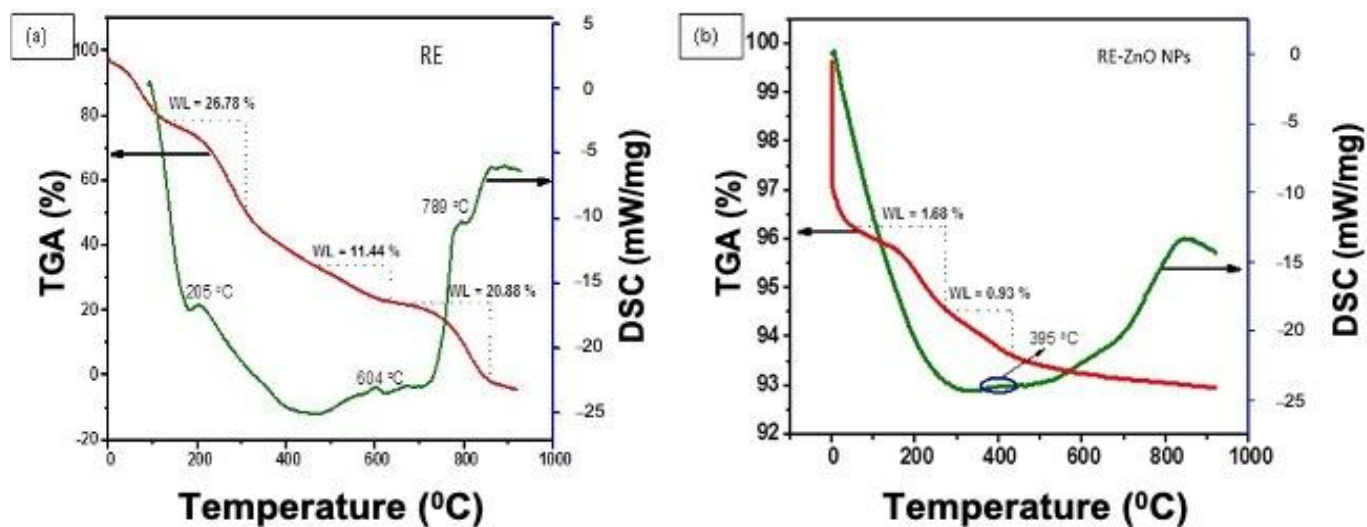


Figure 3. Thermogravimetric analysis spectra of the *R. fairholmianus* root extract (RE) (a) and RE-zinc oxide nanoparticles (RE-ZnO NPs) (b).

Figure 4 describes the XRD pattern of biosynthesized RE-ZnO NPs. The peaks at 2θ 32° , 34° , 36.1° , 46° , 58° , 64° , 66° , 70° , and 72° can be indexed to (100), (101), (102), (110), (103), (200), (112), and (201), planes are matching with those patterns present in the International Center of Diffraction Data card (JCPDS card no: 36-1451), which confirms the crystalline nature of the RE-ZnO NPs. The absence of diffraction peaks showed that the synthesized ZnO NPs are pure without any cross-contamination with other molecules and crystalline in nature. The Debye–Scherrer equation was used to determine the size of the RE-ZnO NPs and showed the size is about 11.34 nm. During the biosynthesis process, the aromatic hydroxyl groups (OH) of *Rubus* interact with zinc ions and leads to the formation of RE-ZnO NPs. The unreacted zinc nitrate precursors and intermediate products were observed as a peak around the 30 nm and 60 nm wavelengths. The particle size of the synthesized ZnO NPs was in close agreement with the previous findings of Fakhari et al. who synthesized the ZnO NPs of an average size of 21.49 nm [39].

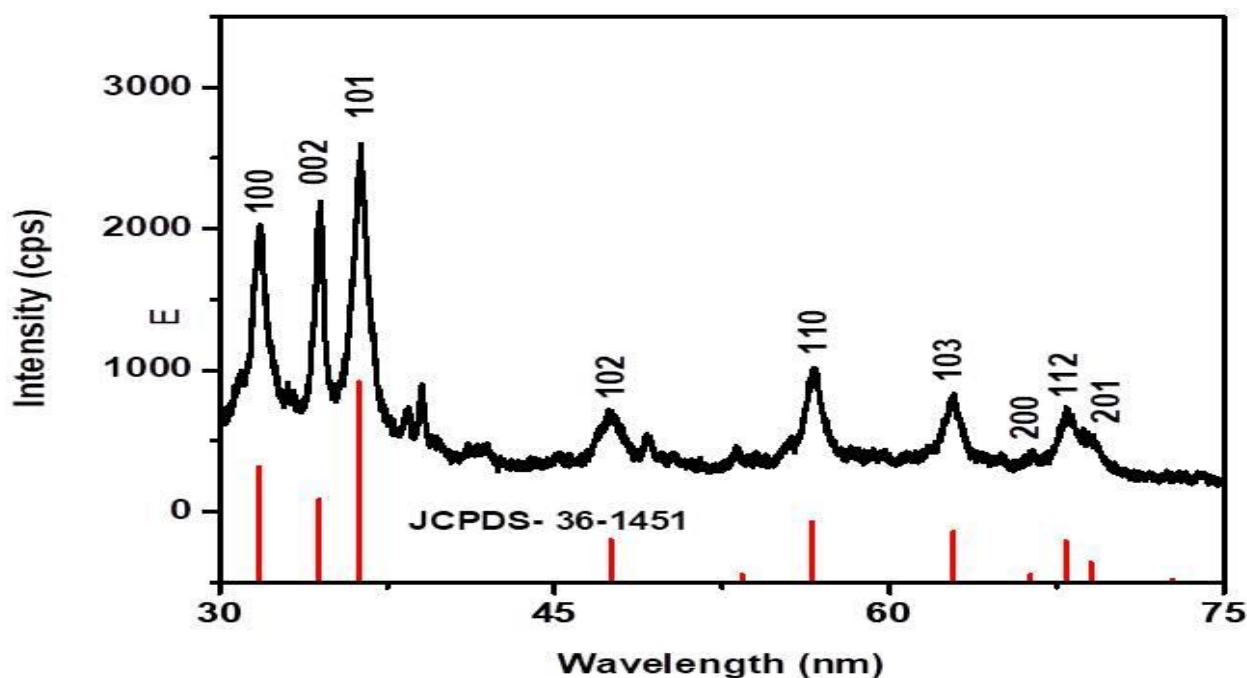


Figure 4. XRD pattern of *R. fairholmianus* root extract (RE) and RE-zinc oxide nanoparticles (RE-ZnO NPs).

Figure 5 displays the SEM image of ZnO NPs synthesized using RE. The excellent distribution of ZnO NPs in RE might be due to the presence of organic compounds in *Rubus*, which facilitates the reduction of zinc nitrate from RE that can offer adequate surface charges between individual ZnO NPs. It was found that the individual particles aggregated together to form larger spherical particles, which were uniformly distributed. The EDAX spectrum shows the presence of Zn and O together with carbon and oxygen, which can be attributed to the extract. The synthesized nanoparticles are aggregated in a spherical shape and showed an average size between 1 and 100 nm. The characterization results obtained in this study were found to be similar to the earlier reports on the biosynthesis of ZnO NPs from algal and other plant extracts [40,41]; however, this is the first report on *R. fairholmianus* mediated green synthesis of ZnO NPs.

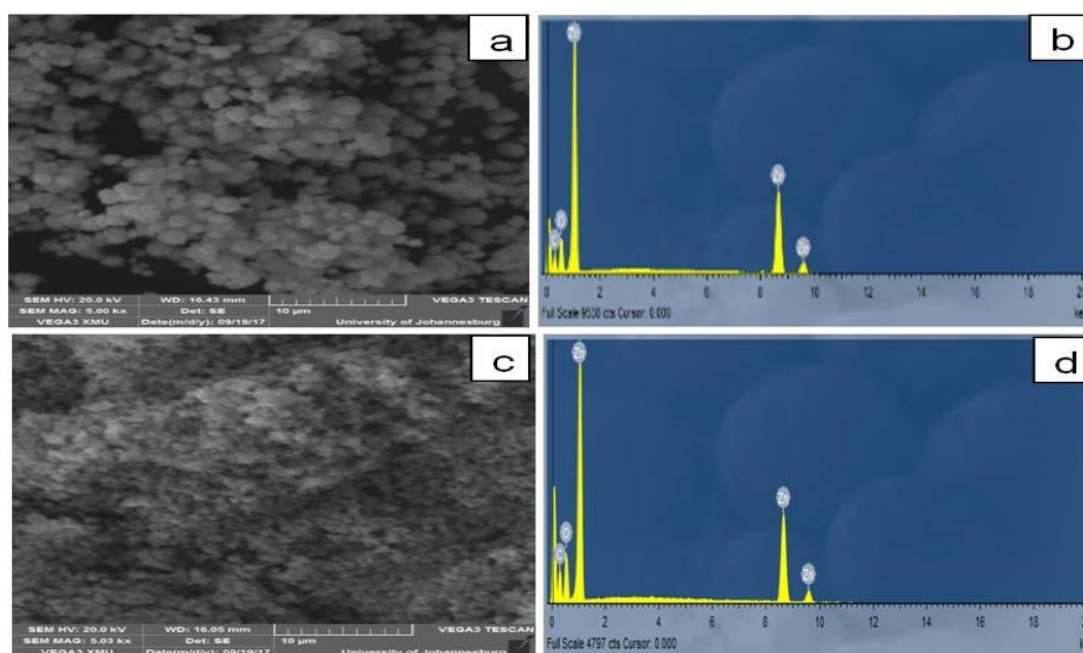


Figure 5. SEM images of RE-zinc oxide nanoparticles (RE-ZnO NPs). (a) RE-ZnO NPs; (b) Spectrum of RE-ZnO NPs; (c) ZnO alone; (d) Spectrum of ZnO alone.

Tables 1 and 2 and Figure 6 depict the antibacterial activity of RE, and RE-ZnO NPs against *S. aureus*. The results indicated that RE and RE-ZnO NPs have antibacterial activities at various concentrations against the target bacteria. RE-ZnO NPs displayed the most significant spectrum of activity. The inhibitory effect of RE-ZnO NPs was observed at 157.22 $\mu\text{g}/\text{mL}$ (MIC), whereas RE was at 337.86 $\mu\text{g}/\text{mL}$ (MIC). Ampicillin showed an inhibitory activity at 0.79 $\mu\text{g}/\text{mL}$ (MIC) on *S. aureus*.

Table 2. Minimum inhibitory concentration (MIC) of *R. fairholmianus* root extract (RE) and RE-zinc oxide nanoparticles (RE-ZnO NPs).

Samples	Susceptibility ($\mu\text{g}/\text{mL}$)
	<i>S. aureus</i>
	MIC
RE	337.86
RE-ZnO NPs	157.22
Ampicillin (positive control)	0.79

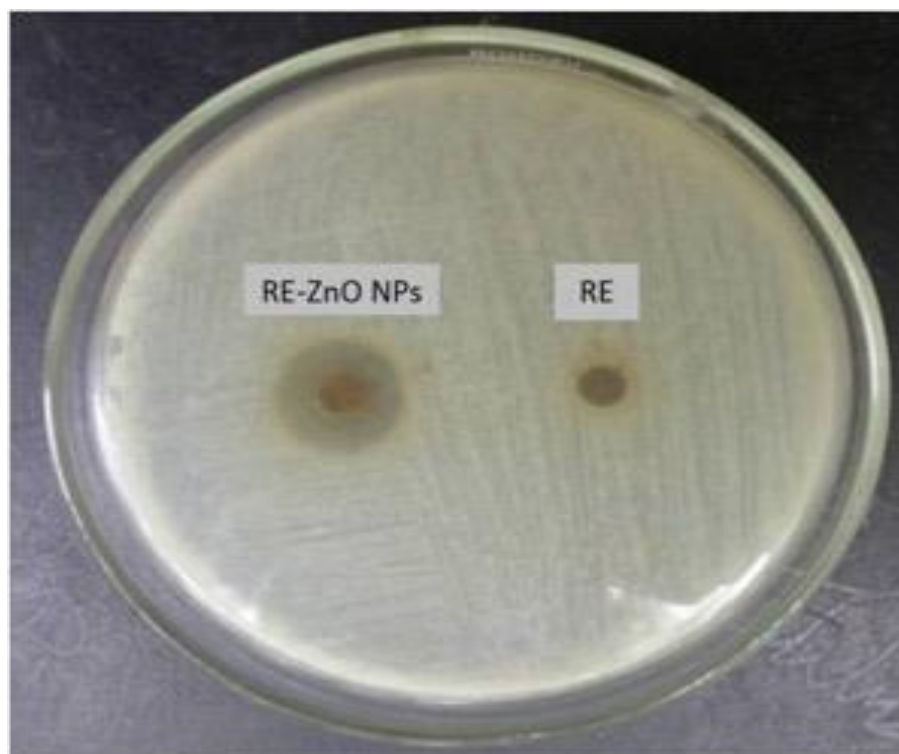


Figure 6. Antibacterial activity of *R. fairholmianus* root extract (RE) and RE-zinc oxide nanoparticles (RE-ZnO NPs) against *S. aureus* in agar well diffusion method.

Table 3 reveals the antibacterial effect of *R. fairholmianus* root extract (RE), and RE-ZnO NPs at various concentrations. The smaller size of the nanoparticles simplifies their entry through the microbial cell membrane, and thereby inhibits cell growth and promotes bacterial cell death. Metal nanoparticles, mainly ZnO NPs, have strong anti-microbial properties; the mechanism behind this is that ZnO NPs will generate hydrogen peroxides (H_2O_2) and these peroxides will disturb the lipid and protein bilayers that lead to the destruction of bacterial cells [42]. The other antimicrobial action of ZnO NPs is that it involves the generation of reactive oxygen species (ROS) and NPs accumulation in the cytoplasm that induces cell death. The generated ROS will damage bacterial proteins, lipids, and DNA to induce cell death [43,44]. Due to the smaller size (1–100 nm), NPs easily breach through the cell wall and enter mitochondria leading to mitochondrial oxidative stress and apoptosis that eventually results in cell death [44]. A recent study by Kumar et al. proved that ZnO NPs prepared with *Raphanus sativus* root extract have excellent antimicrobial activity against MDR strain [45].

Table 3. Bacterial growth in different concentrations of *R. fairholmianus* root extract (RE), and RE-ZnO NPs.

Groups	10 µg/mL	20 µg/mL	30 µg/mL	40 µg/mL	50 µg/mL
RE	+	+	+	+	+
RE-ZnO NPs	+	+	-	-	-
Positive Control	+	+	+	+	+
Negative Control	-	-	-	-	-

Positive (+) = color change (red to yellow) indicating growth of *S. aureus*; Negative (–) = no color change (red) indicating the absence of growth of *S. aureus*.

Previous reports of ZnO NPs from plant extracts showed good antibacterial effects against various pathogenic bacteria. To the best of our knowledge, this is the first study where the *R. fairholmianus* root extract has been used to synthesize ZnO NPs. Plants from

the *Rubus* genus were found to possess flavonoids, tannins, and polyphenolics, which could explain their biological properties and strong antibacterial properties. The different phytochemicals in the *R. fairholmianus* extract are responsible for the reduction of zinc nitrate in the formation of RE-ZnO NPs, and its antibacterial activity against *S. aureus*.

4. Conclusions

In this study, we reported a green and eco-friendly process to synthesize ZnO NPs using *Rubus fairholmianus* root extract. The initial indication of the formation of ZnO NPs is the change in the color of the reaction solution from a brownish-yellow to a pale white. The size of the biosynthesized RE-ZnO NPs is 100 nm and it is confirmed by SEM analysis. The phytochemicals of *R. fairholmianus* were helpful in the formation of ZnO NPs as evidenced by FTIR results. The XRD study showed that the synthesized RE-ZnO NPs were high in purity, and crystalline in nature. The synthesized RE-ZnO NPs showed strong antimicrobial properties. These findings revealed that *R. fairholmianus* could be potentially used in the production of metal nanoparticles for large-scale synthesis.

Author Contributions: Conceptualization, N.K.R. and B.P.G.; methodology, N.K.R.; validation, N.K.R.; B.P.G. and N.N.H.; investigation, N.K.R.; writing—original draft preparation, N.K.R.; writing—review and editing, N.K.R.; N.N.H. and B.P.G.; supervision, project administration, funding acquisition, H.A. and N.N.H. All authors have read and agreed to the published version of the manuscript.

Funding: This work is based on the research supported by the South African Research Chairs Initiative of the Department of Science and Technology and National Research Foundation of South Africa (Grant No 98337).

Institutional Review Board Statement: Not applicable.

Informed Consent Statement: Not applicable.

Data Availability Statement: Not applicable.

Acknowledgments: This work is based on the research supported by the South African Research Chairs Initiative of the Department of Science and Technology and National Research Foundation of South Africa (Grant No 98337). The authors sincerely thank the University of Johannesburg, the National Laser Centre (CSIR-NLC), and the National Research Foundation (NRF) of South Africa for their financial support.

Conflicts of Interest: The authors declare that there is no conflict of interests.

Sample Availability: Not available.

References

1. Sivaraj, R.; Pattanathu, K.; Rajiv, P.; Hasna, S.; Venckatesh, R. Biogenic copper oxide nanoparticles synthesis using *Tabernaemontana divaricate* leaf extract and its antibacterial activity against urinary tract pathogen. *Acta Part A Mol. Biomol. Spectrosc.* **2014**, *133*, 178–181. [[CrossRef](#)] [[PubMed](#)]
2. Rudramurthy, G.R.; Swamy, M.K.; Sinniah, U.R.; Ghasemzadeh, A. Nanoparticles: Alternatives Against Drug-Resistant Pathogenic Microbes. *Molecules* **2016**, *21*, 836–842. [[CrossRef](#)]
3. Hamelian, M.; Zangeneh, M.M.; Amisama, A.; Varmira, K.; Veisi, H. Green synthesis of silver nanoparticles using *Thymus kotschyanus* extract and evaluation of their antioxidant, antibacterial and cytotoxic effects. *Appl. Organomet. Chem.* **2018**, *32*, e4458. [[CrossRef](#)]
4. Hemmati, S.; Rashtiani, A.; Zangeneh, M.M.; Mohammadi, P.; Zangeneh, A.; Veisi, H. Green synthesis and characterization of silver nanoparticles using *Fritillaria* flower extract and their antibacterial activity against some human pathogens. *Polyhedron* **2019**, *158*, 8–14. [[CrossRef](#)]
5. Zangeneh, M.M.; Bovandi, S.; Gharehyakheh, S.; Zangeneh, A.; Irani, P. Green synthesis and chemical characterization of silver nanoparticles obtained using *Allium saralicum* aqueous extract and survey of in vitro antioxidant, cytotoxic, antibacterial and antifungal properties. *Appl. Organomet. Chem.* **2019**. [[CrossRef](#)]
6. Sánchez-López, E.; Gomes, D.; Esteruelas, G.; Bonilla, L.; Lopez-Machado, A.L.; Galindo, R.; Cano, A.; Espina, M.; Ettcheto, M.; Camins, A.; et al. Metal based nanoparticles as antimicrobial agents: An overview. *Nanomaterials* **2020**, *10*, 292. [[CrossRef](#)]

7. Seydi, N.; Mahdavi, B.; Paydarfard, S.; Zangeneh, A.; Zangeneh, M.M.; Najafi, F.; Jalalvand, A.R.; Pirabbasi, E. Preparation, characterization, and assessment of cytotoxicity, antioxidant, antibacterial, antifungal, and cutaneous wound healing properties of titanium nanoparticles using aqueous extract of *Ziziphora clinopodioides* Lam leaves. *Appl. Organomet. Chem.* **2019**, *33*. [[CrossRef](#)]
8. Zhaleh, F.; Zangeneh, A.; Goorani, S.; Seydi, N.; Zangeneh, M.M.; Tahvilian, R.; Pirabbasi, E. In vitro and in vivo evaluation of cytotoxicity, antioxidant, antibacterial, antifungal, and cutaneous wound healing properties of gold nanoparticles produced via a green chemistry synthesis using *Gundelia tournefortii* L. as a capping and reducing agent. *Appl. Organomet. Chem.* **2019**, *33*. [[CrossRef](#)]
9. Zangeneh, M.M.; Joshani, Z.; Zangeneh, A.; Miri, E. Green synthesis of silver nanoparticles using aqueous extract of *Stachys lavandulifolia* flower, and their cytotoxicity, antioxidant, antibacterial and cutaneous wound-healing properties. *Appl. Organomet. Chem.* **2019**, *33*. [[CrossRef](#)]
10. Rouhi, J.; Mahmud, S.; Naderi, N.; Ooi, C.R.; Mahmood, M.R. Physical properties of fish gelatin-based bio-nanocomposite films incorporated with ZnO nanorods. *Nanoscale Res. Lett.* **2013**, *8*, 364–371. [[CrossRef](#)]
11. Kolekar, T.V.; Bandgar, S.; Shirguppikar, S.S.; Ganachari, V.S. Synthesis and characterization of ZnO nanoparticles for efficient gas sensors. *Arch. Appl. Sci. Res.* **2013**, *5*, 20–28.
12. Jayaseelan, C.; Abdul, R.A.; Vishnu, K.A.; Marimuthu, S.; Santhoshkumar, T.; Bagavan, A.; Gaurav, K.; Karthik, L.; Rao, B.K.V. Novel microbial route to synthesize ZnO nanoparticles using *Aeromonas hydrophila* and their activity against pathogenic bacteria and fungi. *Spectrochim. Acta A* **2012**, *90*, 78–84. [[CrossRef](#)] [[PubMed](#)]
13. Sangeetha, G.; Rajeshwari, S.; Venkatesh, R. Green Synthesis of Zinc Oxide Nanoparticles by Aloe Barbadensis Miller Leaf Extract: Structure and Optical Properties. *Mater. Res. Bull.* **2011**, *46*, 2560–2566. [[CrossRef](#)]
14. Gunalan, S.; Sivaraj, R.; Rajendran, V. Green synthesized ZnO nanoparticles against bacterial and fungal pathogens. *Prog. Nat. Sci. Mater. Int.* **2012**, *22*, 693–700. [[CrossRef](#)]
15. Ladj, R.; Bitá, A.; Eissa, M.; Mugnier, Y.; Le Dantec, R.; Fessi, H.; Elaissari, A. Individual inorganic nanoparticles: Preparation, functionalization and in vitro biomedical diagnostic applications. *J. Mater. Chem. B* **2013**, *1*, 1381–1396. [[CrossRef](#)] [[PubMed](#)]
16. Zheng, Y.; Zhang, H.; Fu, L. Preparation gold nanoparticles using herb leaf extract for electro-oxidation determination of ascorbic acid. *Inorg. Nano Met. Chem.* **2018**, *48*, 449–453. [[CrossRef](#)]
17. Zheng, Y.; Huang, Y.; Shi, Y.; Fu, Y. Green biosynthesis of ZnO nanoparticles by *Plectranthus amboinicus* leaf extract and their application for electrochemical determination of norfloxacin. *Inorg. Nano Met. Chem.* **2019**, *49*, 277–282. [[CrossRef](#)]
18. Ying, J.; Zheng, Y.; Zhang, H.; Fu, L. Room temperature biosynthesis of gold nanoparticles with *Lycoris aurea* leaf extract for the electrochemical determination of aspirin. *Rev. Mex. Ing. Quim.* **2020**, *19*, 585–592. [[CrossRef](#)]
19. Jalalvand, A.R.; Zhaleh, M.; Goorani, S.; Zangeneh, M.M.; Seydi, N.; Zangeneh, A.; Moradi, R. Chemical characterization and antioxidant, cytotoxic, antibacterial, and antifungal properties of ethanolic extract of *Allium Saralicum*, R.M. Fritsch leaves rich in linolenic acid, methyl ester. *J. Photochem. Photobiol. B* **2019**, *192*, 103–112. [[CrossRef](#)]
20. Sayyedrostami, T.; Pournaghi, P.; Ebrahimi Vosta-Kalaeae, S.; Zangeneh, M.M. Evaluation of the wound healing activity of *Chenopodium botrys* leaves essential oil in rats (a short-term study). *J. Essent. Oil Bear. Plants* **2018**, *21*, 164–174. [[CrossRef](#)]
21. Zhaleh, M.; Sohrabi, N.; Zangeneh, M.M.; Zangeneh, A.; Moradi, R.; Zhaleh, H. Chemical composition and antibacterial effects of essential oil of *Rhus coriaria* fruits in the west of Iran (Kermanshah). *J. Essent. Oil Bear. Plants* **2018**, *21*, 493–501. [[CrossRef](#)]
22. Othman, L.; Sleiman, A.; Abdel-Massih, R.M. Antimicrobial Activity of Polyphenols and Alkaloids in Middle Eastern Plants. *Front. Microbiol.* **2019**, *10*, 911–920. [[CrossRef](#)]
23. Abbas, M.; Saeed, F.; Anjum, F.M.; Afzaal, M.; Tufail, T.; Bashir, M.S. Natural polyphenols: An overview. *Int. J. Food Prop.* **2017**, *20*, 1689–1699. [[CrossRef](#)]
24. George, B.P.; Thangaraj, P.; Sulaiman, C.; Piramanayagam, S.; Ramaswamy, S.K. Bioassay Directed Isolation and Biological Evaluation of Compounds Isolated from *Rubus fairholmianus* Gard. *Biomed. Res. Int.* **2014**, *204340*, 1–15. [[CrossRef](#)]
25. George, B.P.; Abrahamse, H.; Parimelazhagan, T. Caspase dependent apoptotic inhibition of melanoma and lung cancer cells by tropical *Rubus* extracts. *Biomed. Pharmacother.* **2016**, *80*, 193–199. [[CrossRef](#)]
26. Zheng, Y.; Li, F.; Fuigui, H.; Aiwu, W.; Wen, C.; Jinping, Y.; Feng, P. Green biosynthesis and characterization of zinc oxide nanoparticles using *Corymbia citriodora* leaf extract and their photocatalytic activity. *Green. Chem. Lett. Rev.* **2015**, *8*, 59–63. [[CrossRef](#)]
27. Jayappa, M.; Ramaiah, C.; PavanKumar, M.; Suresh, D.; Prabhu, A.; Devasya, R.; Sheikh, S. Green synthesis of zinc oxide nanoparticles from the leaf, stem and in vitro grown callus of *Mussaenda frondosa* L.: Characterization and their applications. *Appl. Nanosci.* **2020**, *1–8*. [[CrossRef](#)] [[PubMed](#)]
28. Jayachandran, A.; Aswathy, T.R.; Nair, A. Green synthesis and characterization of zinc oxide nanoparticles using *Cayratia pedata* leaf extract. *Biochem. Biophys. Rep.* **2021**, *26*, 100995. [[CrossRef](#)]
29. Barziniy, A.; Azeez, H. Green synthesis and characterization of zinc oxide nanoparticles using *Eucalyptus globulus* Labill. leaf extract and zinc nitrate hexahydrate salt. *SN Appl. Sci.* **2020**, *2*, 991. [[CrossRef](#)]
30. Balogun, S.W.; James, O.; Sanusi, Y.; Olayinka, O. Green synthesis and characterization of zinc oxide nanoparticles using bashful (*Mimosa pudica*), leaf extract: A precursor for organic electronics applications. *SN App. Sci.* **2020**, *2*, 504. [[CrossRef](#)]
31. Pillai, M.; Sivasankarapillai, V.; Rahdar, A.; Joseph, J.; Sadeghfhar, F.; Anu, R. Green synthesis and characterization of zinc oxide nanoparticles with antibacterial and antifungal activity. *J. Mol. Struct.* **2020**, *1211*, 128107. [[CrossRef](#)]

32. Mandell, G.; Douglas, J.; Bennett, R. *Principles and Practice of Infectious Diseases*, 4th ed.; Churchill Livingstone Ltd.: Edinburgh, UK, 1995.
33. Oladiran, A.A.; Olabisi, I.A. Synthesis and characterization of ZnO nanoparticles with zinc chloride as zinc source. *Asian J. Nat. Appl. Sci.* **2013**, *2*, 41–44.
34. Senthilkumar, N.; Nandhakumar, E.; Priya, P.; Soni, C.; Vimalan, M.; Vetha, N. Synthesis of ZnO nanoparticles using leaf extract of *Tectona grandis* (L.) and their anti-bacterial, anti-arthritis, anti-oxidant and in vitro cytotoxicity activities. *New J. Chem.* **2017**, *41*, 10347–10356. [[CrossRef](#)]
35. Tamuly, C.; Hazarika, M.; Borah, S.; Das, M.R.; Boruah, M.P. The synthesis of citrate-modified silver nanoparticles in an aqueous suspension of graphene oxide nanosheets and their antibacterial activity. *Colloids Surf. B Biointerfaces* **2013**, *102*, 627–634. [[CrossRef](#)] [[PubMed](#)]
36. Darezereshki, E.; Alizadeh, M.; Bakhtiari, F.; Schaffie, M.; Ranjbar, M. A novel thermal decomposition method for the synthesis of ZnO nanoparticles from low concentration ZnSO₄ solutions. *Appl. Clay Sci.* **2011**, *54*, 107–111. [[CrossRef](#)]
37. Matinise, N.; Fuku, X.G.; Kaviyarasu, K.; Mayedwa, N.; Maaza, M. ZnO nanoparticles via *Moringa oleifera* green synthesis: Physical properties & mechanism of formation. *Appl. Surf. Sci.* **2017**, *406*, 339–347. [[CrossRef](#)]
38. El-Kader, F.H.A.; Hakeem, N.A.; Elashmawi, I.S.; Ismail, A.M. Structural, optical and thermal characterization of ZnO nanoparticles doped in PEO/PVA blend films. *Nanosci. Nanotechnol.* **2013**, *7*, 179–188.
39. Fakhari, S.; Jamzad, M.; Fard, H.K. Green synthesis of zinc oxide nanoparticles: A comparison. *Green Chem. Lett. Rev.* **2019**, *12*, 19–24. [[CrossRef](#)]
40. Azizi, S.; Ahmad, M.B.; Namvar, F.; Mohamad, R. Green biosynthesis and characterization of zinc oxide nanoparticles using brown marine macroalga *Sargassum muticum* aqueous extract. *Mater. Lett.* **2013**, *116*, 275–277. [[CrossRef](#)]
41. Zhang, L.; Jiang, Y.; Ding, Y.; Daskalakis, K.; Povey, J.L.; O’Neil, A.J. Mechanistic investigation into antibacterial behaviour of suspensions of ZnO nanoparticles against *E. coli*. *J. Nanopart. Res.* **2010**, *12*, 1625–1636. [[CrossRef](#)]
42. Dutta, R.K.; Nenavathu, B.P.; Gangishetty, M.K.; Reddy, A.V.R. Studies on antibacterial activity of ZnO nanoparticles by ROS induced lipid peroxidation. *Colloids Surf. B Biointerfaces* **2012**, *94*, 143–150. [[CrossRef](#)] [[PubMed](#)]
43. Akhtar, M.J.; Ahamed, M.; Kumar, S.; Khan, M.M.; Ahmad, J.; Alrokayan, S.A. Zinc oxide nanoparticles selectively induce apoptosis in human cancer cells through reactive oxygen species. *Int. J. Nanomed.* **2012**, *7*, 845–857. [[CrossRef](#)]
44. Xia, T.; Kovoichich, M.; Nel, A.E. Impairment of mitochondrial function by particulate matter (PM) and their toxic components: Implications for PM-induced cardiovascular and lung disease. *Front. Biosci.* **2007**, *12*, 1238–1246. [[CrossRef](#)] [[PubMed](#)]
45. Kumar, A.B.V.; Saila, E.S.; Narang, P.; Aishwarya, M.; Raina, R.; Gautam, M.; Shankar, E.G. Biofunctionalization and biological synthesis of the ZnO nanoparticles: The effect of *Raphanus sativus* (white radish) root extract on antimicrobial activity against MDR strain for wound healing applications. *Inorg. Chem. Comm.* **2019**, *100*, 101–106. [[CrossRef](#)]